Near-field scanning optical microscopy investigation of immiscibility effects in $In_{1-x}Ga_xP$ films grown by liquid phase epitaxy

C. A. Paulson and A. B. Ellis
Department of Chemistry, University of Wisconsin, Madison, Wisconsin 53706

P. D. Moran and T. F. Kuech[a)]
Department of Chemical Engineering, University of Wisconsin, Madison, Wisconsin 53706

(Received 12 July 2001; accepted for publication 13 November 2001)

Near-field scanning optical microscopy (NSOM) and electron probe microanalysis (EPMA) were used to study the topographic and microscopic optical properties of indium–gallium–phosphide ($In_{1-x}Ga_xP$) samples grown by liquid phase epitaxy on gallium–arsenide substrates. NSOM imaging found strong and highly localized variations in the photoluminescence (PL) intensity for samples that were highly lattice mismatched with the substrate. The topography and optical features were roughly spatially correlated for these samples. Shifts in the PL peak energy position (by as much as 27 meV) were found during scans across highly mismatched samples, whereas no shifts were seen for $In_{1-x}Ga_xP$ films with a nearly lattice matched composition. Compositional fluctuations were determined to be the cause of these PL peak energy shifts. EPMA provided corroborating evidence that compositional fluctuations are spatially correlated with the topography. These composition fluctuations arise from the known solid–solid miscibility gap in the $In_{1-x}Ga_xP$ system at temperatures used for the growth of these samples. © *2002 American Institute of Physics.* [DOI: 10.1063/1.1433184]

INTRODUCTION

Indium–gallium–phosphide ($In_{1-x}Ga_xP$) is an important alloy system that is used in many semiconductor electronic devices. Growth of $In_{1-x}Ga_xP$ is accomplished by a variety of methods, including metalorganic vapor phase epitaxy (MOVPE),[1] molecular beam epitaxy,[2] and liquid phase epitaxy (LPE).[3,4] Among these, LPE is often recognized as having industrial appeal due to its high deposition rate and potentially high purity. LPE deposition occurs under conditions that are close to thermodynamic equilibrium. Under such conditions, immiscibility can be an important parameter for the LPE deposition of semiconductor alloys. Previous work has demonstrated that deposition of alloys that have compositions in the thermodynamic miscibility gap can result in increased dislocation density and increased surface roughness.[5] Fluctuations in local alloy composition can decrease carrier mobility through alloy scattering.[6] Since these effects are detrimental to devices, immiscibility is an important issue to be considered when studying the deposition of these semiconductor materials.

Spatially resolved investigations of composition fluctuations in LPE films have used cathodoluminescence (CL),[7] electron probe microanalysis (EPMA),[8] and transmission electron microscopy (TEM),[8–11] among other techniques. Also there are many investigations of the spatial distributions for impurities in LPE materials, for examples see Refs. 4 and 12. Only a relatively few studies report results on LPE films that have large values of lattice mismatch with their substrates ($\Delta a/a_0 > 0.5\%$).[5,13] Here we present results of near-field scanning optical microscopy (NSOM) investigations of LPE $In_{1-x}Ga_xP$ samples grown on gallium arsenide (GaAs) substrates over a range of lattice mismatch that varied from ~0% to 2%. The NSOM images reveal a high level of local variation in the photoluminescence (PL) spectra when the composition is well removed from the lattice matched composition of $x = 0.51$. The ability of the NSOM experiment to simultaneously determine surface topography along with optical properties demonstrate a spatial correlation between changes in the PL intensity and changes in the surface topography. The PL fluctuations can result from compositional fluctuations or strain in the material.[14,15] By comparison with results from EPMA and x-ray diffraction experiments, the contrast in the NSOM images is shown to result from composition fluctuations in these films. These composition fluctuation results are driven by the known thermodynamic miscibility gap in this alloy system.[1,16,17]

EXPERIMENTAL DETAILS

Samples of $In_{1-x}Ga_xP$ were grown by LPE on ⟨100⟩ GaAs substrates. The average composition for these samples was determined using far-field PL spectroscopy.[5] Samples of $In_{0.49}Ga_{0.51}P$, $In_{0.65}Ga_{0.35}P$, and $In_{0.77}Ga_{0.23}P$ were investigated. These samples have approximately 0%, 1%, and 2% lattice mismatch with the GaAs substrate, respectively.[18] All epitaxial layers were between 1 and 2 μm thick. Far-field collection mode NSOM was performed in an air ambient at room temperature. An argon ion laser was used for the excitation source, and the aperture of the NSOM probe was approximately 50 nm in diameter. Our NSOM instrument uses a parabolic mirror to efficiently gather the luminescence and this is analyzed using a 1/4 m spectrometer and detected by

a)Author to whom correspondence should be addressed; electronic mail: kuech@engr.wisc.edu

a water-cooled photomultiplier tube detector.[19] The spectral resolution was set to 12 meV at the photon energy of 1.7 eV. NSOM imaging was performed with the spectrometer centered at different specific energies, allowing spatially and spectrally resolved data to be obtained from these $In_{1-x}Ga_xP$ materials. Each 8×8 μm^2 NSOM image required approximately 1 h for acquisition.

Spatial mapping of the alloy composition by EPMA was performed using a Cameca SX51 electron microprobe instrument running in x-ray fluorescence imaging mode. For all the microprobe results, the beam current was 80 nA (Faraday current) at 1500 V, and the peak integration time was 30 s. The small local changes in alloy composition necessitated long measurement integration times. A 15×15 μm^2 image was acquired in 5 h. The electron beam excitation area was approximately 1 μm^2, and the pixel spacing was therefore set at 1 μm. During EPMA, the electron beam excites x-ray emission from the atoms in the sample. The energy of the x-ray fluorescence is element specific, being related to the core energy levels in the atoms.[20] The intensity of the x-ray fluorescence is proportional to the concentration in the sample of the element that is fluorescing. The x-ray mapping was performed using the indium *L*, gallium *L*, phosphorus *K*, and arsenic *L* x-ray lines. Control standards of pure InP and GaP were used to calibrate the intensity of x-ray emission from In, Ga, and P atoms. Oxygen, carbon, and silicon were not detected in measurable quantities in the $In_{1-x}Ga_xP$ samples. The elemental totals for In and Ga atoms was slightly below 100% (by a couple of percentage points), as compared with the P counts, but no other elements were found to compensate for the absence of In and Ga atoms. This slightly low total may be due to small differences in the x-ray fluorescence yield between the calibration standards, InP and GaP, and the unknown $In_{1-x}Ga_xP$ samples.[20] Since $In_{1-x}Ga_xP$ is a stoichiometric compound, In and Ga alone account for 100% of the electropositive elements present in the solid, and therefore the elemental totals for In and Ga were normalized to 100%. After normalization, the slightly low totals also gave a small discrepancy between the compositions determined from EPMA and those determined from PL, with the difference being one or two percentage points. However, this article deals with relative changes in the composition of the semiconductor. Since the measurements were very repeatable, the slight discrepancy described above does not compromise the integrity of the conclusions presented below.

These samples were also investigated by atomic force microscopy (AFM) operating in contact mode, and by scanning electron microscopy (SEM). The x-ray diffraction θ–2θ measurements were performed using a Bede x-ray diffractometer.

RESULTS

NSOM was used to gather 8×8 μm^2 images of the topography and optical properties of all three LPE samples. A topographic image gathered during NSOM of the ~1% lattice-mismatched $In_{0.65}Ga_{0.35}P$ sample is shown in Fig. 1(a). Generally, the bright and dark areas of the image (representing peaks and valleys in the topography, respectively) occur along a diagonal connecting the upper right to the lower left corner of the image. The PL peak energy was found to vary between 1.676 and 1.703 eV when probed at different areas across this sample, as discussed below. Therefore, luminescence intensity imaging was performed with the spectrometer centered on energies within this range. NSOM PL intensity images are shown in Figs. 1(b) and 1(c). These were acquired with the spectrometer centered at 1.703 and 1.676 eV, respectively. The PL intensity image gathered at 1.703 eV [Fig. 1(b)] was repeated several times, from the same area, with all of the resulting images being nearly identical. The topography remained unchanged for all the images, at all energies, indicating that the tip did not drift significantly between scans. The spatial variation in the luminescence images show bright and dark areas that occur along the diagonal connecting the upper right to the lower left corner of the image, indicating that there is a similar spatial distribution for the luminescence intensity when compared to features in the topography image.

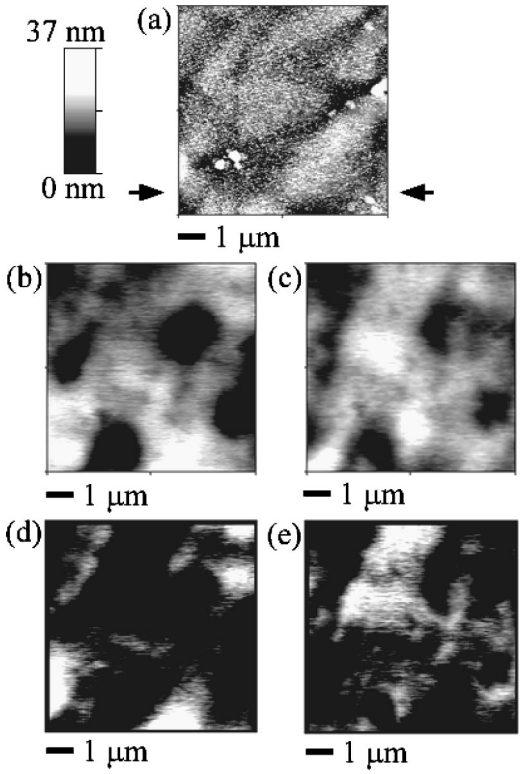

FIG. 1. NSOM images from the $In_{0.65}Ga_{0.35}P$ sample, all from the same 8×8 μm^2 region. (a) Topography. The gray scale ranges from 0 to 37 nm. Arrows next to this image indicate a line along which point spectroscopy was performed. (b) An image of PL intensity at 1.703 eV. The gray scale represents a 12-fold change in the luminescence signal magnitude. (c) An image of PL intensity at 1.676 eV with the gray scale representing a sixfold change in the luminescence signal magnitude. (d) This image results from the subtraction of image (c) from image (b), highlighting areas that strongly luminesce at 1.703 eV. (e) This image results from the subtraction of image (b) from image (c), highlighting areas that strongly luminesce at 1.676 eV.

The images gathered at 1.703 and 1.676 eV [Figs. 1(b) and 1(c), respectively] show clear differences in their spatial distributions of luminescence intensity. These images were processed to have the same brightness scales. Then the im-

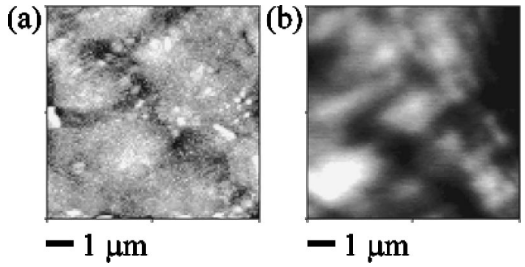

FIG. 2. NSOM 8×8 μm^2 images from the $In_{0.77}Ga_{0.23}P$ sample. (a) Topography. The gray scale ranges from 0 to 33 nm. (b) An image of PL intensity at 1.55 eV. The gray scale represents a 16-fold change in the luminescence signal magnitude.

ages were carefully overlaid, and the difference between the images was determined by subtracting the brightness values of one image from those of the other image. The resulting images are shown in Figs. 1(d) and 1(e). The bright regions in Fig. 1(d) correspond to regions of strong luminescence at 1.703 eV [bright in Fig. 1(b)] while having simultaneously weak luminescence at 1.676 eV [dark in Fig. 1(c)]. The bright regions in Fig. 1(e) correspond to regions that have strong luminescence at 1.676 eV and simultaneously weak luminescence at 1.703 eV.

NSOM imaging was also performed on the $In_{0.77}Ga_{0.23}P$ (2% lattice mismatch) and the $In_{0.49}Ga_{0.51}P$ (nearly lattice-matched) LPE samples. A representative NSOM image of the $In_{0.77}Ga_{0.23}P$ sample is presented in Fig. 2. In the topographic image, shown in Fig. 2(a), an extended valley (dark region) appears along a diagonal that extends from the upper left corner of the image to the lower right corner. In the luminescence image of the band edge PL intensity at 1.55 eV [Fig. 2(b)], several features are seen that roughly occur along this same diagonal. The NSOM images of the nearly lattice-matched $In_{0.49}Ga_{0.51}P$ sample are not shown. This sample exhibited a relatively smooth morphology when compared to the lattice-mismatched samples, and only a very weak spatial variation was found in the luminescence intensity.

Point spectroscopy was performed on the $In_{0.65}Ga_{0.35}P$ sample. During point spectroscopy, the NSOM tip is held at a fixed position over the sample while a PL spectrum is recorded. Fourteen point spectra are shown in Fig. 3. These were acquired from points roughly evenly separated by ~0.5 μm, along a line that is indicated by arrows in Fig. 1(a). The energy at the center of the PL peak ranged between the minimum of 1.676 eV in spectrum 10, to the maximum of 1.703 eV in spectrum 5. Changes in the magnitude of the PL peak maximum are also seen in these PL point spectra.

EPMA was used to perform x-ray fluorescence imaging of the spatial distributions of In and Ga in the $In_{1-x}Ga_xP$ samples. Results from the x-ray fluorescence imaging of the $In_{0.65}Ga_{0.35}P$ sample are shown in Fig. 4. An optical microscope image, 70×70 μm^2 in size, is shown in Fig. 4(a). This image was taken from the area surrounding the area where the EPMA images were gathered, and was taken before the EPMA mapping was performed. Carbon was deposited by the electron beam during the EPMA measurement, and could easily be seen in the optical microscope after EPMA had been performed. This carbon spot was used to identify the

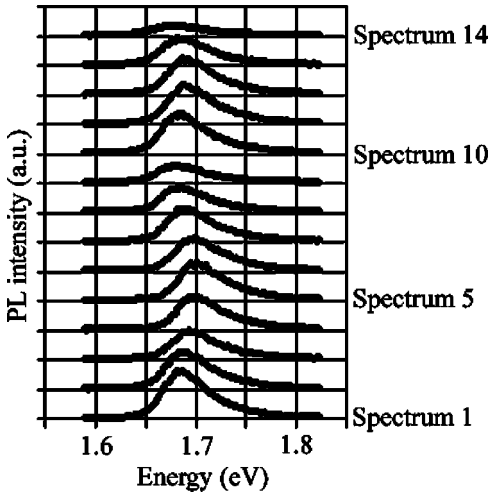

FIG. 3. Fourteen PL point spectra gathered from the $In_{0.65}Ga_{0.35}P$ sample of Fig. 1. These point spectra were evenly spaced along the line indicated by arrows in Fig. 1(a), starting at the left of the image (spectrum 1) and proceeding to the right (spectrum 14). The peak maximum ranged from 1.676 to 1.703 eV for these spectra. All of the spectra were recorded at the same sensitivity so that their intensities can be directly compared.

exact measurement area. A box (15×15 μm^2 in size) in the optical microscope image [Fig. 4(a)] indicates the area that was probed by the electron beam. The distribution of the Ga atomic percentage, within the box of Fig. 4(a), and determined from the EPMA x-ray fluorescence imaging, is shown in Fig. 4(b); and the corresponding x- ray fluorescence image of the In distribution is shown in Fig. 4(c). Each of the x-ray fluorescence images is 15×15 μm^2 in size, nearly four times the area of the NSOM images, which were 8×8 μm^2 in size. Bright areas in the EPMA x-ray fluorescence images indicate a higher atomic percentage of Ga, in Fig. 4(b), or of In, in Fig. 4(c). X-ray mapping was also performed for the ele-

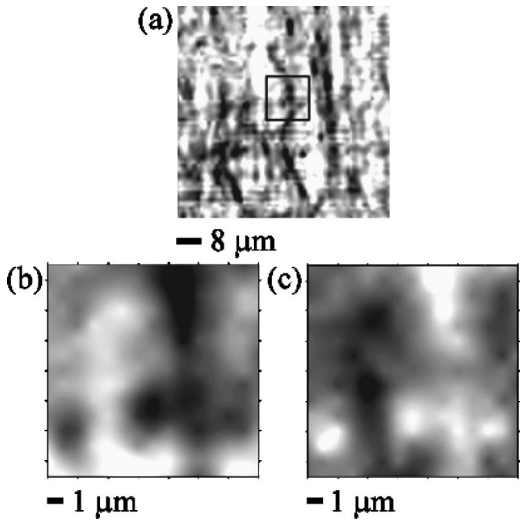

FIG. 4. Nomarskii microscope and electron microprobe images of the LPE $In_{0.65}Ga_{0.35}P$ sample. (a) A 70×70 μm^2 optical microscope image of the region investigated by EPMA. The square marked in this image indicates the area that was interrogated by the electron beam. (b) A 15×15 μm^2 image of the Ga atomic percentage. Light areas have a higher Ga atomic percentage. (c) A 15×15 μm^2 image of the In atomic percentage. Light areas have a higher In atomic percentage.

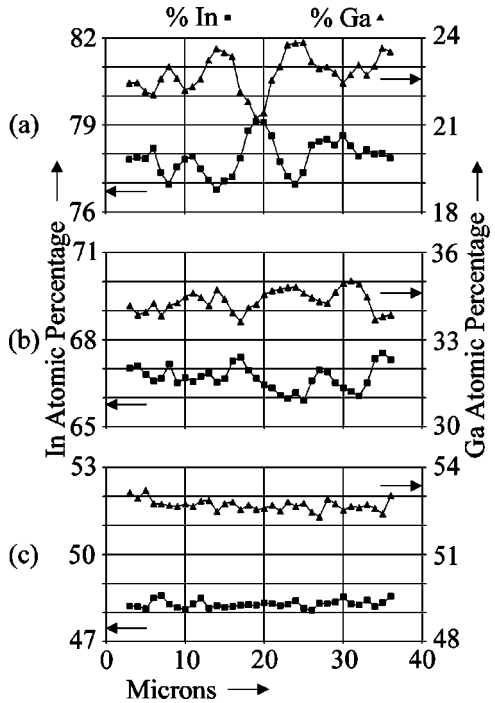

FIG. 5. 34 μm long EPMA line scans revealing quantitative changes in gallium and indium atomic percentages across $In_{1-x}Ga_xP$ samples. (a) $In_{0.77}Ga_{0.23}P$, (b) $In_{0.65}Ga_{0.35}P$, and (c) $In_{0.49}Ga_{0.51}P$. In all cases, the vertical line spacing on the charts represents a change in atomic percentage by one percentage point.

ments phosphorus and arsenic, the only other elements known to be present in the heterostructure, but no trends were noted for their distributions. For the two lattice-mismatched samples, it was clear that the Ga atomic percent is high where the In atomic percent is low, indicating their respective atomic percentages change in an inversely correlated fashion. This result is expected based on the fixed stoichiometry of the alloy. The totals for In and Ga always remained approximately constant.

The magnitude of the compositional fluctuations (measured in the number of percentage points of In or Ga composition) was different for the three samples. The magnitude of the gallium and indium compositional fluctuations is effectively illustrated by electron microprobe line scans across these samples. Representative line scans are shown in Fig. 5. These line scans are each 34 μm long. The samples are labeled on the left-hand side of the figure with their PL-derived compositions. There is a slight discrepancy between the composition determined by EPMA, and that determined by PL, as was discussed in the Experimental Details of this article. From Fig. 5 we clearly see that the largest changes in atomic percentages are observed for scans across the $In_{0.77}Ga_{0.23}P$ sample [Fig. 5(a)], where the percentage of gallium and indium changed by 2–3 percentage points on going across the line scan. Further, it is clear that the gallium and indium compositions are highly correlated spatially. Line scans across the $In_{0.65}Ga_{0.35}P$ sample [Fig. 5(b)] also show that the Ga and In atomic percentages are correlated, but the magnitude of the atomic percentage change is reduced to only 1–2 percentage points. For the $In_{0.49}Ga_{0.51}P$ sample, the changes in atomic percent are less than 1 percentage point, and uncorrelated to within the detection limit of the experiment.

The surface topography was also investigated using AFM and SEM (neither one is shown here). Both techniques gave images of the surface topography that were very similar to those gathered using the NSOM, with surface depressions occurring in extended trenches along the surface. The AFM also gave a similar scale for the surface features, which varied in height by a few tens of nanometers.

X-ray diffraction in θ–2θ mode was performed on the $In_{0.65}Ga_{0.35}P$ sample. Results from the (004) diffraction peak indicate a lattice constant for the $\langle 001 \rangle$ direction of 5.742 $\pm$0.003 Å. The full width at half maximum (FWHM) was 1120 arcsec. The error bar was calculated using 1/10 of the FWHM of the diffraction peak.

DISCUSSION

In all NSOM experiments, it is important to determine the source of contrast recorded during imaging.[21] In the present measurements, both the PL peak intensity and the energy value for the PL peak position were found to vary as function of spatial position across the $In_{0.65}Ga_{0.35}P$ sample, as shown in Fig. 3. The PL peak energy position can change as a result of either strain in the material or changes in the alloy composition.[14,15] Since the epitaxial layers were all greater than 1 μm in thickness, they are all totally or near to totally strain-relaxed.[22] Fully relaxed $In_{0.65}Ga_{0.35}P$ is predicted to have a lattice constant of 5.731 Å by Vegard's law.[18] The measured lattice constant, 5.742$\pm$0.003 Å, is in reasonable agreement with the relaxed value. If the film was under compressive strain, the measured lattice constant would be closer to the GaAs lattice constant, 5.653 Å. Therefore, the variation in spatially resolved PL intensity images, as seen by the NSOM experiments described above, are attributed to fluctuations in the alloy composition.

The composition fluctuations quantified by the electron microprobe experiment corroborate well with this interpretation. Consider the NSOM point spectroscopy results of Fig. 3, where the highest PL peak energy value was 1.703 eV, and the lowest PL peak energy value was 1.676 eV. For $In_{1-x}Ga_xP$, the band edge emission energy varies with composition[5] as determined by Eq. (1)

$$h\nu = 1.35 + 0.73x + 0.70x^2. \tag{1}$$

Using this expression, the PL peak energy-derived composition varies between the average compositions of $In_{0.64}Ga_{0.36}P$ and $In_{0.66}Ga_{0.34}P$. The composition therefore fluctuates with a maximum Δx of about 2 percentage points. This is in reasonable agreement with the corresponding microprobe result, which shows a maximum composition fluctuation Δx of about 1.5 percentage points for the $In_{0.65}Ga_{0.35}P$ sample, as seen in Fig. 5(b).

The features in Figs. 1(d) and 1(e) can now be interpreted. The bright areas in Fig. 1(d) correspond to Ga-rich areas with a band gap close to 1.703 eV, and a composition near $In_{0.64}Ga_{0.36}P$. Likewise, the bright areas in Fig. 1(e) are In-rich areas, with a band gap close to 1.676 eV, and an average composition near $In_{0.66}Ga_{0.34}P$. Several of these fea-

tures seen in the images of the In- and Ga-rich areas, Figs. 1(d) and 1(e), are roughly correlated with surface depressions (dark regions) that are seen in the topography image, Fig. 1(a).

There are several models discussing the possible origins of the spatial fluctuations in the composition. Many investigations, e.g., Refs. 7 and 12 and references in Refs. 3 and 4, have based a mechanism on fluctuations in the rate of incorporation of material into the growing film, which lead to spatial compositional variations in LPE-deposited material. This mechanism focuses on the equilibrium elemental distribution coefficients and spatial fluctuations in the step velocities during growth across different regions of the sample. The distribution coefficient is defined as the ratio of the composition in the solid phase to that in growth media, and can be different for each element that is being deposited, but is constrained by stoichiometry. In regions that have a high step velocity, and therefore high growth rate, the local growth media at the growth interface becomes depleted of the elements that have large distribution coefficients. The local growth rate is rapid and the medium near the growth front becomes depleted of these elements. In regions of low step density or velocity that are growing more slowly, the ambient is not depleted locally of elements with high distribution coefficients. Local variations in the step structure therefore result in composition fluctuations across the deposited film.

This mechanism was used to explain the results of the study by Kato *et al.*,[7] where they used CL to study LPE-grown $In_{1-x}Ga_xAs_{1-y}P_y$ materials. They found increased atomic percentages (by up to 1%) for Ga and P, for ''off-facet'' regions relative to ''on-facet'' regions, surrounding an approximately 100 μm diam, circular, smooth facet. The facet was relatively tall, standing 1–4 μm high, as compared to the surrounding film. Their measurements were made with 5 μm spatial resolution.

Such a mechanism could also be present in our study of $In_{1-x}Ga_xP$ leading to the observed composition fluctuations. In general, the distribution coefficient during LPE is greater, for smaller atoms such as Ga and P, as compared to larger atoms, such as In and As,[23] as shown in Refs. 7 and 24. The distribution coefficients for In and Ga are therefore expected to be different in this study, with Ga having a higher value. A local difference in vertical growth velocity in the LPE materials studied here is evident by the measured NSOM topography image, where the peaks and valleys differ in height by tens of nanometers. This local difference in growth rate is related to the change in the incorporation rate with the high step density associated with this topology.

The EPMA results, shown in Fig. 4, provide clear evidence of a correlation between the composition and topographic features. For the NSOM results, the composition and topography are only roughly correlated [see Figs. 1(a), 1(d), and 1(e)], having features that occur along similar spatial directions in the material. However, in both cases a correlation exists between the composition and the topology, supporting a mechanism in which changes in the local growth velocity leads to variation in composition.

The driving force for compositional fluctuations is the tendency for phase separation due to the growth of materials within the known miscibility gap in the $In_{1-x}Ga_xP$ system.[9,16] The immicibility driven phase separation can lead to the formation of both Ga- and In-rich areas. The growth interface, with the high diffusivity in the liquid growth ambient, can provide an energetically favorable location for this phase separation to occur. These thermodynamic driving forces combine with the changes in step velocity to yield spatial composition variations.

With regard to the dark (non-radiative) areas seen in Figs. 1(b), 1(c), and 2(b); in a previous study it was found that as the lattice mismatch is increased, for heteroepitaxial films deposited by LPE, the morphology becomes rougher, and the dislocation density increased [5]. Dislocations are known to decrease radiative efficiency in these semiconductor systems.[15] The non-radiative regions in the NSOM images [Figs. 1(b), 1(c), and 2(b)] are most likely related to dislocations in the materials. Nonradiative areas were found on both the $In_{0.65}Ga_{0.35}P$ and $In_{0.77}Ga_{0.23}P$ samples (1% and 2% lattice mismatch, respectively), but were not found on the near lattice-matched samples. The contrast in the NSOM images was also found to increase with increasing mismatch for our samples. This means that the areas with lower radiative efficiency became relatively darker, when compared with the radiative areas of the sample, as the degree of mismatch increased in these materials, most likely due to an increased dislocation density.

EPMA measurement on samples with a nominal composition of $In_{0.65}Ga_{0.35}P$ grown by metalorganic chemical vapor deposition (MOCVD) on GaAs substrates exhibited similar spatial fluctuations in the In and Ga atomic percentages to those that were reported here for the LPE- grown samples.

The spatial resolution is limited by electron bloom in the material during the EPMA experiment. The bloom is usually several microns in size. The smaller scale features seen in the NSOM images were therefore not observed by EPMA. The NSOM measurements demonstrated superior spatial resolution, since the smallest features found in Fig. 1(c) are about 250 nm in their minimum spatial dimension. Also, NSOM does not require a vacuum ambient, unlike EPMA. The NSOM measures shifts in the PL peak energy and these shifts can be due to alloy composition and strain. The combination of x-ray diffraction and EPMA was therefore used to confirm that the observed PL shifts were due to compositional variations in the present study. Since the ultimate resolution in the NSOM experiment is limited by the size of the aperture,[20] which was approximately 50 nm for these experiments, higher spatial resolution in the NSOM images of these alloy fluctuations could result from improvements in the PL signal-to-noise ratio.

CONCLUSIONS

NSOM and EPMA were used to spatially quantify composition fluctuations in $In_{1-x}Ga_xP$ heterostructures grown by LPE on GaAs substrates. Alloy composition fluctuations were correlated with changes in surface topography, where features in the composition fluctuations have a similar spatial distribution to features seen in the surface topography. Immiscibility provides a driving force for this alloy fluctuation

under common growth conditions. NSOM provided higher resolution images of the composition fluctuations than EPMA, with greater sensitivity to alloy composition, and provides an alternative method for probing the local composition changes in a broad class of metastable semiconductor materials.

ACKNOWLEDGMENTS

The authors thank John Fournelle for assistance with the EPMA measurements and Nelson Tansu for the MOCVD samples. Financial support from the Army Research Office and Office of Naval Research is gratefully acknowledged, as is the support of the UW-Materials Research Science and Engineering Center (MRSEC) funded by the National Science Foundation.

[1] G. B. Stringfellow, *Organometallic Vapor Phase Epitaxy, Theory and Practice* (Academic, New York, 1989).
[2] S. F. Yoon, K. W. Mah, and H. Q. Zheng, J. Alloys Compd. **280**, 299 (1998).
[3] M. B. Small, E. A. Giess, and R. Ghez, in *Handbook of Crystal Growth*, edited by D. T. J. Hurle (Elsevier, New York, 1994), Vol. 3.
[4] E. Bauser, in *Handbook of Crystal Growth*, edited by D. T. J. Hurle (Elsevier, New York, 1994).
[5] G. B. Stringfellow, J. Appl. Phys. **43**, 3455 (1972).
[6] T. W. Kim, H. J. Ko, and H. L. Park, Solid State Commun. **110**, 29 (1999).
[7] T. Kato, T. Matsumoto, and T. Ishida, Jpn. J. Appl. Phys., Part 1 **28**, 1513 (1989).
[8] P. Henoc, A. Izrael, M. Quillec, and H. Launois, Appl. Phys. Lett. **40**, 963 (1982).
[9] A. G. Norman and G. R. Booker, J. Appl. Phys. **57**, 4715 (1985).
[10] O. Ueda, S. Isozumi, and S. Komiya, Jpn. J. Appl. Phys., Part 2 **23**, L241 (1984).
[11] J. P. Gowers, Appl. Phys. A: Solids Surf. **31**, 23 (1983).
[12] T. Nishinaga, C. Sasaoka, and K. Pak, Jpn. J. Appl. Phys., Part 1 **28**, 836 (1989).
[13] T. F. Kuech and J. O. McCaldin, J. Vac. Sci. Technol. **17**, 891 (1980).
[14] L. B. Chang, K. Y. Cheng, and C. C. Liu, Cryst. Res. Technol. **24**, 213 (1989).
[15] G. D. Gilliland, Mater. Sci. Eng., R. **R18**, 99 (1997).
[16] B. de Cremoux, P. Hirtz, and J. Ricciardi, Inst. Phys. Conf. Ser. **56**, 115 (1981).
[17] G. B. Stringfellow, J. Cryst. Growth **58**, 194 (1982).
[18] A. Onton, M. R. Lorenz, and W. Reuter, J. Appl. Phys. **42**, 3420 (1971).
[19] J. Liu, N. R. Perkins, M. N. Horton, J. M. Redwing, A. Tischler, and T. F. Kuech, Appl. Phys. Lett. **69**, 3519 (1996).
[20] L. E. Murr, *Electron and Ion Microscopy and Microanalysis* (Marcel Dekker, New York, 1982).
[21] M. A. Paesler and P. J. Moyer, *Near-field Optics, Theory, Instrumentation and Applications* (Wiley, New York, 1996).
[22] J. W. Matthews, A. E. Blakeslee, and S. Mader, Thin Solid Films **33**, 253 (1976).
[23] P. D. Greene, *The Chemistry of the Semiconductor Industry*, edited by S.J. Moss and A. Ledwith (Blackie, London, 1987).
[24] M. Feng, T. H. Windhorn, M. M. Tashima, G. E. Stillman, Appl. Phys. Lett. **32**, 758 (1978).